Front. Optoelectron. 2018, 11(2): 107–115
https://doi.org/10.1007/s12200-018-0802-4

REVIEW ARTICLE

Broadband linearization for 5G fronthaul transmission

Xiupu ZHANG (✉)

iPhotonics Labs, Department of Electrical and Computer Engineering, Concordia University, Montreal, Quebec, H3G1M8, Canada

Abstract 5G is emerging, but the current fronthaul transmission technologies used for 3G and 4G may not be efficient and appropriate for 5G. It has been found that frequency division multiple access (FDMA) and time-division multiple access (TDMA) based radio over fiber (RoF) may be considered the most appropriate for 5G fronthaul transmission technology. Due to analog RoF transmission, broadband linearization is required. In this work, both electrical and optical broadband linearization techniques are reviewed.

Keywords 5G, fronthaul, radio over fiber (RoF), optical fiber communications, linearization

1 Introduction

Broadband mobile services have been emerging very rapidly. To address the broadband, long-term evolution (LTE) and LTE Advanced (LTE-A) have been standardized and commercially deployed as 4th generation mobile technology, i.e., 4G. The 4G with LTE and LTE-A supports data rate of 300 Mb/s and 4 Gb/s, respectively [1]. It is known that the 5th generation mobile technology, i.e., 5G, is being developed to realize access speed of 10 Gb/s and above [1,2].

Optical fiber access networks have been used for supporting mobile fronthaul and mobile backhaul to realize cloud radio access networks (C-RAN). The fronthaul is the key element in the C-RAN architecture, as it connects centralized baseband units (BBUs) with remote radio units (RRUs). In the near future, the fronthaul is required to support massive multiple-input multiple-output (MIMO) for 5G [3]. Moreover, common public radio interface (CPRI) for fronthaul has been used, and Ethernet CPRI, i.e., eCPRI, could be used for 5G, which is digitized in-phase (I) and quadrature (Q) waveforms of wireless signals [1]. When binary on-off keying (OOK) optical fiber transmission is used for fronthaul, CPRI introduces inefficient utilization of optical bandwidth. For current 3G and 4G with LTE, cost-effect digital fiber optic transmission meets requirement of CPRI supported fronthaul as wireless data rate is not high; however, for LTE-A and 5G this may not be true. For an example, carrier aggregated five of 20 MHz LTE-A wireless signals with 8×8 MIMO and three directional sector antennas give 147.5 Gb/s CPRI data rate [4]. For the future 5G, carrier aggregation from 5 to 32 wireless signals may be required, and thus the CPRI and even eCPRI data rate becomes very high. To support this high data rate fronthaul, a large number of high speed optical fiber OOK transmission systems are required, making optical/wireless access networks very complicated and cost ineffective.

To achieve bandwidth-efficient mobile fronthaul transmission, several transmission techniques have been proposed and demonstrated, including frequency division multiple access (FDMA) based radio over fiber (RoF) transmission [4,5], time-division multiple access (TDMA) based RoF transmission [6], and the others [5], in which both FDMA and TDMA RoF, called digital signal processing (DSP) assisted RoF [7], are considered the most popular fronthaul transmission techniques [6]. Recently, real-time CPRI compatible TDMA RoF fronthaul transmission of 256 Gb/s was achieved using 10-GHz optics [8]. Therefore, RoF has very strong potential adoption for 5G fronthaul transmission.

Not like digital optical transmission, RoF is based on optical subcarrier modulation (SCM) and it is an analog transmission. Accompanying optical SCM, nonlinear distortion, such as harmonic and intermodulation distortion, is introduced, which induces crosstalk between wireless carriers. The nonlinearities that induce the nonlinear distortion stem from mainly optical transmitters and receivers. For example, a semiconductor laser, which is used for optical transmitters and has a nonlinear relation between driving the bias current and output optical power, will induce various harmonic and intermodulation distortion between aggregated wireless carriers, and also the

Received January 12, 2018; accepted March 15, 2018

E-mail: xzhang@ece.concordia.ca

Invited Paper, Special Issue—Photonics Research in Canada

distortion may overlap with the wireless signals, inducing crosstalk. Consequently, broadband linearization techniques are required for RoF transmission [9]. The linearization means that the nonlinear distortion is suppressed and thus spurious free dynamic range (SFDR) is improved, which is used to represent the distance between signal and nonlinear distortion radio frequency (RF) power.

In this paper, we review the recent progress of broadband linearization techniques for broadband RoF transmission that has potential to be used for emerging 5G fronthaul transmission.

2 Broadband linearization techniques

Figure 1 shows the linearization techniques recently developed, including optical and electrical linearization. The optical and electrical linearization mean the implementation in optical and electrical domain, respectively. Next, we briefly review some techniques given in Fig. 1.

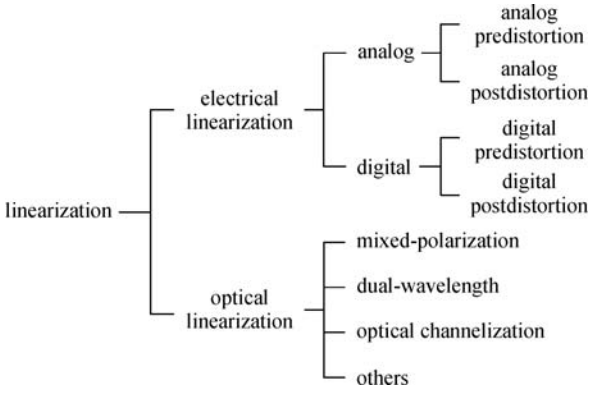

Fig. 1 Linearization techniques [9]

2.1 Electrical linearization

The electrical linearization includes analog and digital predistortion and postdistortion. The pre-/post-distortion means that distortion circuits are located in before/after RoF transmission. As a rule of thumb, predistortion is much more efficient than postdistortion, and therefore the predistortion techniques are only reviewed here. In the following, we review the recent accomplishments in analog predistortion and digital predistortion.

2.1.1 Analog predistortion

An RoF transmission system can be considered a black box, thus a function between input and output RF can be obtained, and the function is usually nonlinear and it can be expanded into a Taylor series. The Taylor series will include 1st, 2nd, 3rd, 4th and 5th order, and further higher orders are usually negligible. The 1st order contains transmitted wireless signals, and the others are called nonlinearities that can induce nonlinear distortion, such as harmonic distortion (HD) and intermodulation distortion (IMD). When the wireless signal bands are not very broad, nonlinear distortion generated by 2nd and 4th order nonlinearities is usually out of the signal bands, thus no degradation is induced by these nonlinearities. This suggests that only 3rd and 5th order nonlinearity induce nonlinear distortion. However, when the wireless signal bands are broad, 2nd and 4th order nonlinearities may generate nonlinear distortion components that are located inside the signal bands in addition to 3rd and 5th order nonlinearity. For example, the wireless signal is ranged from -1.5 to 1.5 GHz in relative frequency [4], some HD and IMD components generated by 2nd order nonlinearity are inside of the signal bands. However, analog predistortion circuits have been designed only for suppressing nonlinear distortion generated by 3rd and 5th order nonlinearity [10–13].

To illustrate the operation principle of analog predistortion, we consider a case of wireless signals having two frequency bands with carriers f_1 and f_2, as shown in Fig. 2. For simplicity, we only consider 3rd order nonlinearity of RoF transmission. Due to the 3rd nonlinearity of RoF transmission, two IMD components at $2f_1-f_2$ and $2f_2-f_1$ are generated at the output when the wireless signals at f_1 and f_2 are transmitted over the RoF, the two red/solid arrows as shown in Fig. 2. Note these two IMD components have the opposite phase to the wireless signals. When an analog predistortion circuit is inserted before the RoF, opposite 3rd and/or 5th order nonlinearity are introduced to the RoF. In other words, when the two wireless signals at f_1 and f_2 are transmitted to the analog predistortion circuit and then RoF, two IMD components at $2f_1-f_2$ and $2f_2-f_1$, indicated by the green/dashed arrows in Fig. 2, are also generated, but they have the opposite phase to the two IMD components generated by the RoF itself. Thus, the IMD components at $2f_1-f_2$ and $2f_2-f_1$, generated by the RoF and analog predistortion circuit, are cancelled out by each other through tuning the bias current of the analog predistortion circuit (APDC). As a rule of thumb, all other components that are generated by 3rd order nonlinearity can be suppressed by the same principle.

As shown in Fig. 3, when 3rd order nonlinearity is only considered, the relation between the input and output of APDC is given by $V_{\text{in}} = a_1 V_{\text{RF}} + a_3 V_{\text{RF}}^3$, where the coefficients a_k, $k = 1$ and 3, are related to the circuit and bias voltage. Similarly, the relation between the input and output of RoF transmission is given by $V_{\text{out}} = b_1 V_{\text{in}} + b_2 V_{\text{in}}^2 + b_3 V_{\text{in}}^3$, where the coefficients b_k, $k = 1$, 2 and 3, are determined by the RoF transmission, where further higher orders are not considered. Thus, the output of the RoF is given by

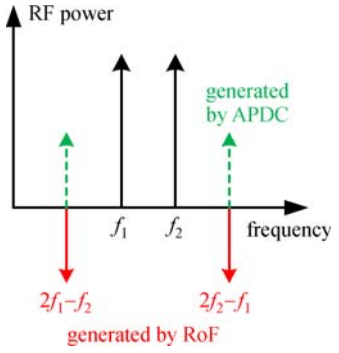

Fig. 2 Working principle of APDC [12]

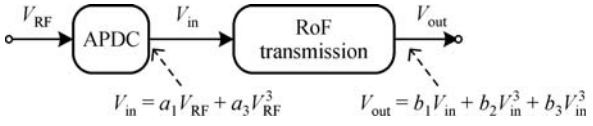

Fig. 3 Mathematic model for APDC to be used for suppression of 3rd order nonlinearity [9]

$$V_{\text{out}} = a_1b_1V_{\text{RF}} + a_1^2b_2V_{\text{RF}}^2 + (a_3b_1 + a_1^3b_3)V_{\text{RF}}^3.$$

To remove the 3rd term means $a_3b_1 + a_1^3b_3 = 0$. If the coefficients of analog predistortion circuit can meet the above condition, the 3rd order nonlinearity of RoF transmission can be removed completely.

It is found that Schottky diodes have opposite nonlinear characteristics to RoF transmission. We have designed a simple analog predistortion circuit that has bandwidth from 3.1 to 4.8 GHz and resulted in SFDR improvement of 11 dB [10]. Later, the circuit was further improved in design. The first improved design is shown in Fig. 4 [11]. Two zero bias GaAs beam lead detector diodes and capacitors were used in the APDC. The diodes can be biased at lower than 3 mA due to zero bias characteristic so that power consumption is very small. No broadband matching network is required because of high series resistance of the zero bias diodes. The anti-parallel structure of the circuit eliminates even order nonlinearity generated by the two diodes. As shown in Fig. 5 that is measured S_{21} versus input RF power to the APDC, it is seen that the S_{21} is increased with the increase of input RF power. It is well known that RoF S_{21} is decreased with the increase of input RF power, a common behavior as almost all RF functional components such as RF amplifiers. This suggests that the APDC has almost opposite response to RoF transmission in S_{21}. Further, the 3rd order nonlinearity, which can induce RoF S_{21} decrease, will be suppressed by the APDC. The circuit has 3-dB bandwidth from 7 to 18 GHz. Using this APDC in an RoF transmission, measured SFDR was improved by more than ~10 dB from 7 to 14 GHz and ~6 dB from 15 to 18 GHz, limited by 5th order nonlinear distortion [11].

The APDC was further improved as shown in Fig. 6 [12], where the dual diode is a three-port chip and the two diodes are connected in anti-parallel. The two diodes are in an anti-parallel structure, so even order nonlinear distortion terms are suppressed at the output of the APDC. The APDC has a 3-dB bandwidth from 10 MHz to 33 GHz. Using this circuit in an RoF transmission system, 3rd order IMD (IMD3) power versus frequency spacing was measured using two RF signals for two cases, as shown in Fig. 7 [12]. By comparison of the two cases, it is seen that the IMD3 is suppressed by more than 10 dB, and the frequency location of the IMD3 does not affect the suppression seriously. It was found that this APDC resulted in a SFDR improvement of ~12 dB for linearizing a directly modulated RoF transmission. To linearize an externally modulated RoF transmission, SFDR was improved by 5 – 12 dB. For a 20-MHz orthogonal frequency division multiplexing (OFDM) WiFi wireless signal at 2.4 GHz, error vector magnitude (EVM) was improved by 3.5 dB for an RoF over 20 km standard single mode fiber (SMF).

The above two analog predistortion circuits only enable to suppress 3rd order nonlinearity, and thus the SFDR of RoF transmission is usually limited by 5th order nonlinearity. Intuitively, further improvement of SFDR requires to suppress 5th order nonlinearity. For this case, similar to Fig. 3 the predistortion circuit output is given by

$$V_{\text{in}} = a_1V_{\text{RF}} + a_3V_{\text{RF}}^3 + a_5V_{\text{RF}}^5.$$

When a RoF system up to fifth order nonlinearity is considered, i.e.,

$$V_{\text{out}} = b_1V_{\text{in}} + b_2V_{\text{in}}^2 + b_3V_{\text{in}}^3 + b_4V_{\text{in}}^4 + b_5V_{\text{in}}^5,$$

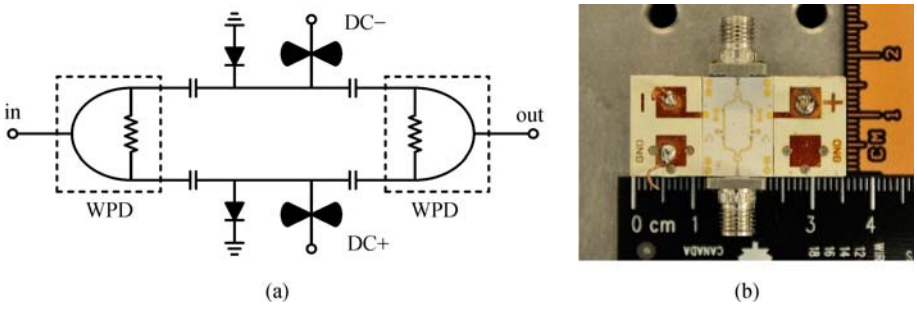

Fig. 4 (a) Schematic of APDC, WPD: Wilkinson power divider; and (b) fabricated APDC [11]

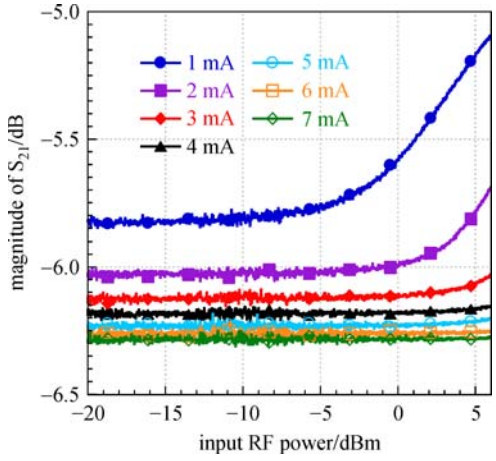

Fig. 5 Measured amplitude modulation/amplitude modulation characteristic of APDC [11]

the output of RoF transmission is given by

$$V_{\text{out}} = a_1 b_1 V_{\text{RF}} + a_1^2 b_2 V_{\text{RF}}^2 + (a_3 b_1 + a_1^3 b_3) V_{\text{RF}}^3 + (a_1^4 b_4 + 2 a_1 a_3 b_2) V_{\text{RF}}^4 + (a_5 b_1 + 3 a_1^2 a_3 b_3 + a_1^5 b_5) V_{\text{RF}}^5.$$

Thus, to suppress both 3rd and 5th order nonlinearity, these conditions must be satisfied, $a_3 b_1 + a_1^3 b_3 = 0$, and $a_5 b_1 + 3 a_1^2 a_3 b_3 + a_1^5 b_5 = 0$. Since the coefficients b_1, b_2, b_3, b_4, and b_5 are fixed for a given RoF transmission, the analog predistortion circuit coefficients a_1, a_3 and a_5 can be tuned to meet the above two conditions. Figure 8 shows our designed analog predistortion circuit for suppression of both 3rd and 5th order nonlinearity [13]. The circuit has a 3-dB bandwidth of 6 GHz. For the above WiFi wireless signal, measured EVM improvement is shown in Fig. 9 for an RoF transmission without fiber and with 10 km SMF transmission.

2.1.2 Digital predistortion

Digital predistortion (DPD) for RF power amplifiers has been investigated for decades [14]. Basically, the DPD has been realized in baseband, and also the DPD models become extremely complicated when the wireless bands are more than three or broadband. We have proposed and demonstrated a simple DPD model that is envelope assisted RF DPD [15]. When the carrier aggregation is enabled, the signal bandwidth can reach 100 MHz or more, which means that the baseband sampling rate of the analog to digital converter (ADC) can be 500 MHz or more. When the memory polynomial works at such a high sampling rate, the memory depth of the DPD might be too long, and thus the number of the polynomial coefficients becomes much higher, in particular when there is a strong long-term memory effect in RoF systems [14]. To tackle this problem, an envelope-assisted RF memory polynomial was proposed, which can be described by

$$z(n) = \Sigma_{j=1}^{J} \Sigma_{p=0}^{P} a_{jp} x(n-p) |x(n-p)|^{j-1} + \Sigma_{k=1}^{K} \Sigma_{q=1}^{Q} b_{kq} x(n) |w(n-q)|^{k-1},$$

where $x(n)$ is the value of wireless signals in RF domain, $w(n)$ is the value of the baseband wireless signal envelopes, J and P are the nonlinear order and memory depth for the wireless signals in RF domain, respectively, K and Q are the nonlinear order and memory depth for the wireless signals in baseband domain, respectively, and a_{jp} and b_{kq} are the model coefficients for the RF and baseband wireless signals, respectively. The first part of the above equation is aimed to eliminate the out-of-band nonlinearities, in-band nonlinearities and short-term memory effect, which are owing to the RF wireless signals, while the second part is aimed to eliminate the in-band nonlinearities and long-term memory effect, which are owing to the baseband wireless signals. The more details of the model can be found in Ref. [15], and the model was verified by two-band and three bands of wireless signals over RoF transmission [15].

When two bands at 800 and 840 MHz, and each band with 20 MHz LTE signal are considered, the RF spectrum after an RoF transmission with 8-km SMF, in which the envelope assisted RF DPD was used, is shown in Fig. 10. For comparison, the conventional two-dimensional DPD (2D-DPD) [16] was also used in the same RoF transmission. It is seen that both in-band and out-of-band

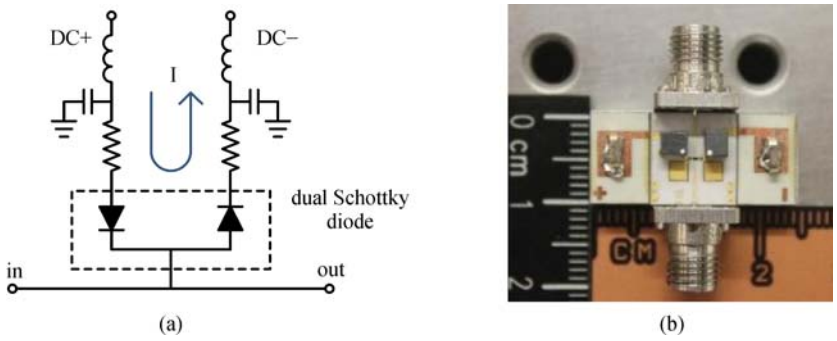

Fig. 6 (a) Schematic of APDC; and (b) photo of APDC [12]

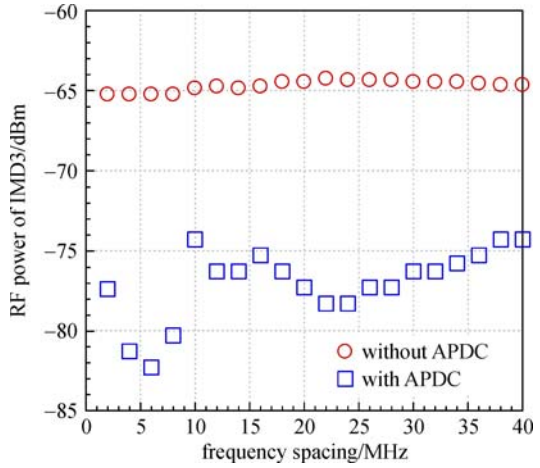

Fig. 7 Measured RF power of IMD3 versus frequency spacing between two RF signals [12]

performance are better for using the envelope assisted RF DPD than that for using the conventional 2D-DPD. Measured EVM shows more improvement of 1.9 dB using the envelope assisted RF DPD than the 2D-DPD.

When the model is used for more than two-bands, such as three bands of wireless signals, baseband DPD models as given in Ref. [14] become very complicated and are difficult to be used. However, the envelope assisted RF DPD model is still very simple. Figure 11 shows measured RF spectrum for three wireless bands at 800, 850 and 900 MHz with LTE signal over RoF transmission [15]. It is seen that the envelope assisted RF DPD is very effective in improvement of in-band and out-of-band performance.

To decrease the sampling bandwidth, the RF wireless signals are down-converted to intermediate frequency (IF) signals, which contain all the bands in frequency domain. Then, the down-converted IF signals can be sampled with a much lower sampling rate. Figure 12 shows the measured output spectrum for envelope assisted IF DPD implemented with a sampling bandwidth of 600 MHz, from 550 to 1150 MHz. For comparison, the performance of the RoF linearized by envelope assisted RF DPD is also shown in

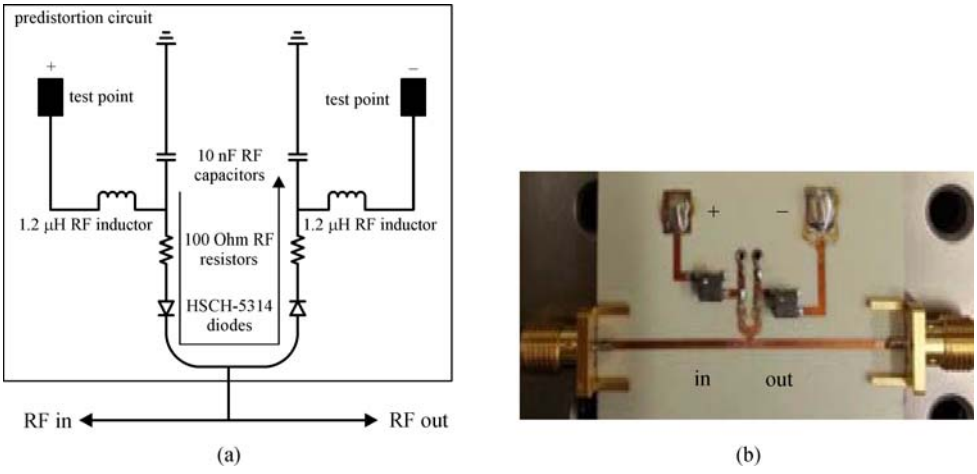

Fig. 8 (a) Schematic of analog predistortion circuit; and (b) photo of designed circuit [13]

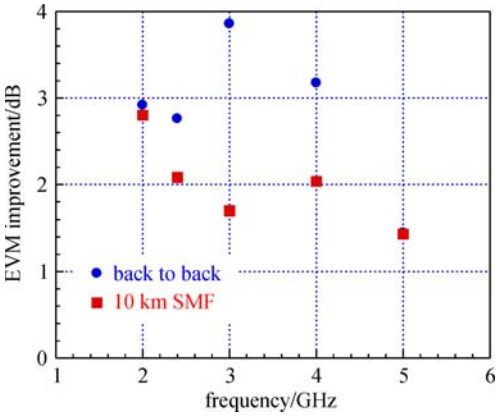

Fig. 9 Measured EVM improvement for WiFi signal with wireless carrier from 2 to 5 GHz over RoF [13]

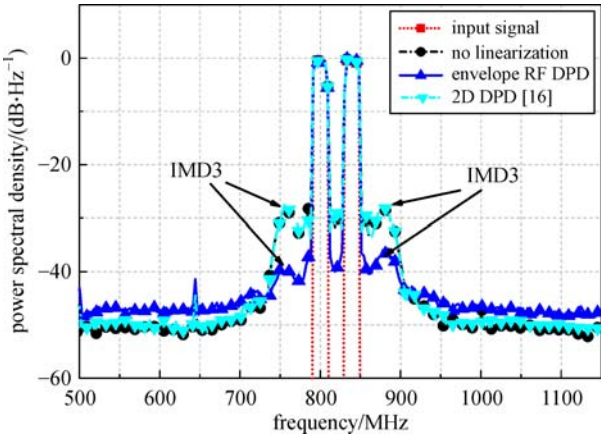

Fig. 10 Measured RF spectrum for two wireless bands at 800 and 840 MHz over RoF [15]

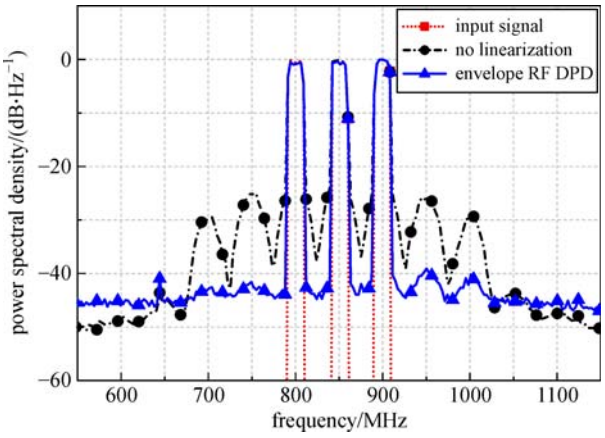

Fig. 11 Measured RF spectrum for three bands of wireless signals at 800, 850 and 900 MHz over RoF transmission [15]

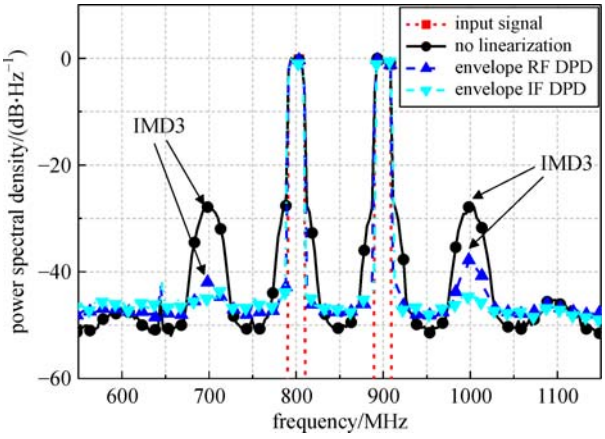

Fig. 12 Measured RF spectrum for two wireless signals at 800 and 900 MHz over RoF [15]

Table 1 Number of coefficients vs memory depth

memory depth*	1	2	3	4	5	6	7	8
envelope DPD**	14	23	32	41	50	59	68	77
2D DPD [16]	30	45	60	75	90	105	120	135

* Suppose nonlinearity order is 5.
** Suppose lengths of RF memory effect and baseband memory effect are equal.

Fig. 12. It is seen that the envelope assisted IF DPD results in a better performance.

Moreover, the complexity of the envelope assisted DPD model in terms of model coefficients is compared to the conventional 2D-DPD and given in Table 1. It is seen that the envelope assisted DPD has about a half of the coefficients compared with the conventional 2D-DPD.

The APDC has features: simple and compact structure, low power consumption and much more broadband, in comparison with the DPD that has features: high complex structure, high power consumption and much narrower band. Moreover, the DPD is highly efficient in in-band distortion suppression, and is difficult in out-of-band distortion suppression. In contrast, the APDC is broadband and thus is able to suppress both in-band and out-of-band distortion. In addition, the memory effect that induces signal distortion can be suppressed only by the DPD, which is very important for broadband signals. In brief, the APDC and DPD are complementary in nonlinear distortion suppression. We have also studied analog and digital predistortion combined linearization for RoF transmission, to utilize the complementary advantages of APDC and DPD, i.e., hybrid APDC and DPD [17]. For two bands of 20 MHz LTE signals transmission over RoF for the cases of without linearization, 2D-DPD [16], APDC, and combined of APDC and 2D-DPD, i.e., hybrid, Fig. 13 shows the output RF spectrum. It is seen that the combined linearization suppresses both in-band and out-of-band distortion, better than either APDC or 2D-DPD.

Table 2 summarizes comparison of three linearization techniques for three scenarios experimentally in improvement of EVM, adjacent channel power ratio (ACPR) and IMD3 [17]. Scenario 2 is the same as for Fig. 13. For Scenario 1, two wireless RF signals are located in 800 and 900 MHz. For Scenario 2, two wireless RF signals are

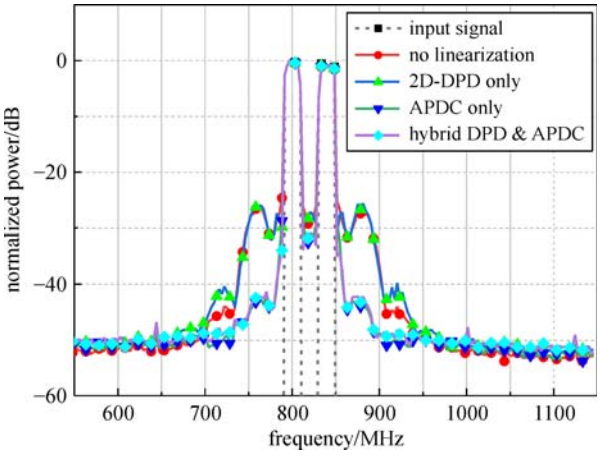

Fig. 13 Measured RF spectrum at the output of RoF transmission that is linearized by either non linearization, 2D-DPD [16], APDC, and hybrid APDC and 2D-DPD. Two RF signals are located at 800 and 840 MHz [17]

located in 800 and 840 MHz. For Scenario 3, three wireless RF signals are located in 800, 850 and 900 MHz. Each band of wireless RF signals is 64 quadrature amplitude modulation (QAM)-OFDM 20 MHz LTE.

2.2 Optical linearization

As a rule of thumb, optical linearization is mainly used to linearize optical components, such as lasers, and optical modulators etc. As shown in Fig. 1, various optical linearization techniques have been investigated. However, mixed polarization and dual-wavelength linearization are considered to have a simple configuration. The principle of the optical linearization is almost similar, namely the nonlinear distortion generated by an optical component at two operation points can cancel each other. Therefore, optical linearization can be used to suppress both second- and third-order nonlinearity as well as further higher order [9].

2.2.1 Mixed polarization linearization

The mixed-polarization linearization means that the nonlinear distortion generated by TE and TM transmission of an optical component is cancelled by each other, when the TE and TM components are mixed to a certain degree and the nonlinear distortion from the TE and TM transmission is out of phase. Therefore, the TE and TM transmission characteristics must be different, which means that the optical component must be polarization dependent, such as polarization dependent Mach-Zehnder modulator (MZM) [18–20] or electro-absorption modulator (EAM) [21,22]. To illustrate the principle, we consider to linearize an MZM that is usually biased at quadrature and has nonlinear transmission, as shown in Fig. 14. The linearized MZM consists of a front and rear polarization linearizer located at its input and output, respectively. The two polarization angles α and β are dependent on TE and TM transmission characteristics of the MZM. The rear polarization linearizer can be replaced by a saturated semiconductor optical amplifier (SOA) [23]. The nonlinear distortion can be significantly suppressed by appropriately adjusting two polarization angles, and the suppression is strongly dependent on the TE and TM transmission characteristics of the MZM or EAM. For example, when GaAs MZM is used, the TE and TM transmission characteristics, which have opposite phase modulation indices, result in much better suppression [24,25]. When an $LiNbO_3$ MZM is linearized by the mixed polarization, Fig. 15 shows the transmission characteristics, in which three cases are given: conventional MZM, MZM linearized by the mixed polarization only, and MZM linearized by the mixed polarization and also saturated SOA. It is seen that the MZM transmission is not sinusoidal anymore and becomes linear with driving voltage. Typically speaking, SFDR improvement by mixed-polarization is more than 10 dB [18–20]. Because of linearization implemented in optical domain, the linearization bandwidth is only limited by optical modulator modulation bandwidth.

Applying for the above mixed polarization linearization, integrated linear optical modulators can be obtained.

2.2.2 Dual-wavelength linearization

The principle of dual-wavelength linearization (DWL) means that the nonlinear distortion generated at two wavelengths λ_A and λ_B can cancel each other [26]. This suggests that an optical component, such as an EAM, must have wavelength dependent transmission characteristics. The nonlinear distortion generated at λ_A and λ_B can be suppressed if they are anti-phase each other. Figure 16 shows a schematic of dual-wavelength RoF transmission, where EAM has nonlinear transmission characteristic and also wavelength dependent. It was found that the suppression of nth order nonlinear distortion must satisfy

$$\frac{P_A \times m_{n\_A}}{P_B \times m_{n\_B}} = -\cos[n\omega_{RF}(DL\Delta\lambda + \Delta t)],$$

Table 2 Comparison of improvements by three linearization techniques

Scenario	linearization method	improvement		
		EVM	ACPR	IMD3
800 and 900 MHz	APDC only	2.0 dB	1.8 dB	14.9 dB
	2D-DPD only	9.9 dB	17.5 dB	0.3 dB
	hybrid	11.0 dB	19.4 dB	15.0 dB
800 and 840 MHz	APDC only	2.2 dB	4.7 dB	17.0 dB
	2D-DPD only	7.0 dB	-0.3dB	-1.1 dB
	hybrid	8.2 dB	4.6 dB	16.8 dB
800, 850 and 900 MHz	APDC only	2.4 dB	3.3 dB	3.7 dB
	RF DPD only	9.3 dB	8.2 dB	16.5 dB
	hybrid	10.1 dB	8.6 dB	16.9 dB

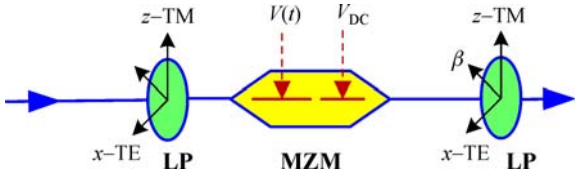

Fig. 14 Schematic of mixed polarization that is used to linearize an MZM. LP: linear polarizer [18]

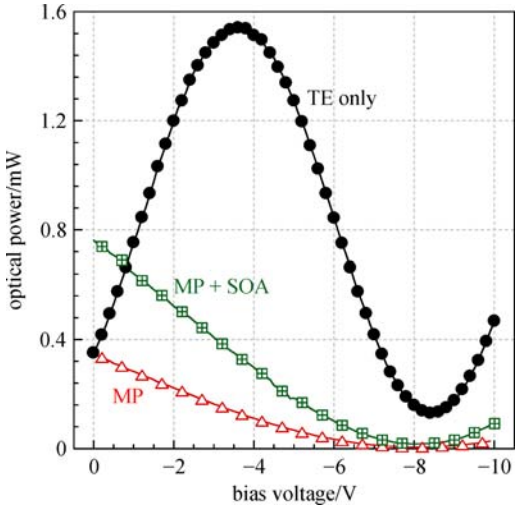

Fig. 15 Measured transmission characteristics for three cases: conventional MZM without linearization (TE only), MZM linearized by mixed-polarization (MP), and MZM linearized by MP combined with a saturated SOA (MP + SOA) [23]

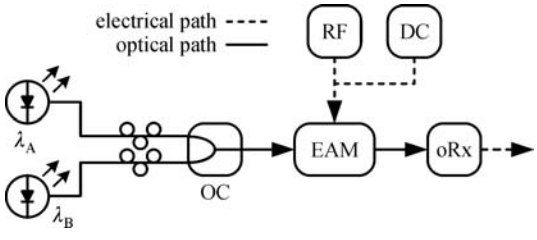

Fig. 16 Schematic of dual-wavelength RoF transmission system. oRx: optical receiver [26]

where P_A and P_B are optical power of λ_A and λ_B, respectively, m_{n_A} and m_{n_B} are the nth order coefficient of Taylor series expansion of the EAM transmission characteristics at λ_A and λ_B, respectively, DL is product of fiber chromatic dispersion and fiber length, $\Delta\lambda = \lambda_B - \lambda_A$, and Δt is the delay induced by chirp of the EAM [26]. It is seen that the suppression of any order nonlinear distortion is dependent on the power ratio of the two wavelengths and the phase of $DL\Delta\lambda + \Delta t$. The linearization was verified using WiFi signals at 2.4 and 5 GHz, 3.5 dB at 2.4 GHz and 2.8 dB at 5 GHz improvements obtained with λ_A = 1510 nm and λ_B = 1552.6 nm [26].

3 Conclusion

We have reviewed our very recent accomplishments of broadband linearization for broadband RoF transmission, including analog predistortion circuit, digital predistortion, mixed polarization and dual-wavelength linearization techniques. Optical linearization is broadband and much desired for linearizing optical components, and also optical linearization can be integrated with the optical components. Analog predistortion circuit can be broadband, but it is less efficient. Digital predistortion is difficult for broadband, but it is efficient for 20 MHz band or less wireless signals. Consequently, electrical and optical linearization can be combined to be used for enhancing linearization in the future.

References

1. Third generation partnership project (3GPP) releases 10-15, 2011–2017
2. Asai T. 5G radio access network and its requirements on mobile optical networks. In: Proceedings of International Conference on Optical Network Design and Modeling (ONDM). Pisa, Italy, 2015, 7–11
3. Larsson E, Edfors O, Tufvesson F, Marzetta T. Massive MIMO for next generation wireless systems. IEEE Communications Magazine, 2014, 52(2): 74–80
4. Liu X, Zeng H, Chand N, Effenberger F. Efficient mobile fronthaul via DSP-based channel aggregation. Journal of Lightwave Technology, 2016, 34(6): 1556–1564
5. Liu X, Effenberger F. Emerging optical access network technologies for 5G wireless. Journal of Optical Communications and Networking, 2016, 8(12): B70–B79
6. Zeng H, Liu X, Megeed S, Chand N, Effenberger F. Real-time demonstration of CPRI compatible efficient mobile fronthaul using FPGA. Journal of Lightwave Technology, 2017, 35(6): 1241–1247
7. Kani J, Terada J, Suzuki K, Otaka A. Solutions for future mobile fronthaul and access network convergence. Journal of Lightwave Technology, 2017, 35(3): 527–534
8. Liu X, Zeng H, Chand N, Effenberger F. CPRI compatible efficient mobile fronthaul transmission via equalized TDMA achieving 256 Gb/s CPRI equivalent data rate in a single 10-GHz bandwidth IM-DD channel. In: Proceedings of Optical Fiber Communications (OFC) Conference. Anaheim, CA, 2016, Paper W1H.3
9. Zhang X, Zhu R, Shen D, Liu T. Linearization technologies for broadband radio-over-fiber transmission systems. MDPI Photonics, 2014, 1(1): 455–472
10. Shen Y, Hraimel B, Zhang X, Cowan G, Wu K, Liu T. A novel analog broadband RF predistortion circuit to linearize electro-absorption modulator in multiband OFDM ultra-wideband radio over fiber systems. IEEE Transactions on Microwave Theory and Techniques, 2010, 58(11): 3327–3335
11. Zhu R, Zhang X, Shen D, Liu T. Broadband analog predistortion circuit using zero bias detector diodes for radio over fiber systems.

IEEE Photonics Technology Letters, 2013, 25(21): 2101–2104
12. Zhu R, Zhang X, Shen D, Zhang Y. Ultra broadband predistortion circuit for radio-over-fiber transmission systems. Journal of Lightwave Technology, 2016, 34(22): 5137–5145
13. Zhang X, Saha S, Zhu R, Liu T, Shen D. Analog pre-distortion circuit for radio over fiber transmission. IEEE Photonics Technology Letters, 2016, 28(22): 2541–2544
14. Wood J. Behavioral Modeling and Linearization of RF Power Amplifiers. Boston: Artech House, 2014
15. Tang W. Envelope-assisted RF digital predistortion for broadband radio-over-fiber transmission with RF amplifier. Dissertation for the Master Degree. Montreal: Concordia University, 2017
16. Bassam S, Helaoui M, Ghannouchi F. 2-D digital predistortion (2-D-DPD) architecture for concurrent dual-band transmitters. IEEE Transactions on Microwave Theory and Techniques, 2011, 59(10): 2547–2553
17. Xie X. Combined linearization of both analog and digital predistortion for broadband radio over fiber transmission. Dissertation for the Master Degree. Montreal: Concordia University, 2017
18. Masella B, Hraimel B, Zhang X. Enhanced spurious-free dynamic range using mixed polarization in optical single sideband Mach-Zehnder modulator. Journal of Lightwave Technology, 2009, 27 (15): 3034–3041
19. Hraimel B, Zhang X. Characterization and compensation of AM-AM and AM-PM distortion in mixed polarization radio over fiber systems. In: Proceedings of IEEE/MTT-S International Microwave Symposium Digest . Montreal, QC, 2012, 1–3
20. Hraimel B, Zhang X, Liu T, Xu T, Nie Q, Shen D. Performance enhancement of an OFDM ultra-wideband transmission-over-fiber link using a linearized mixed-polarization single-drive X-cut Mach-Zehnder modulator. IEEE Transactions on Microwave Theory and Techniques, 2012, 60(10): 3328–3338
21. Hraimel B, Zhang X, Jiang W, Wu K, Liu T, Xu T, Nie Q, Xu K. Experimental demonstration of mixed-polarization to linearize electro-absorption modulators in radio-over-fiber links. IEEE Photonics Technology Letters, 2011, 23(4): 230–232
22. Hraimel B, Zhang X. Performance improvement of radio-over fiber links using mixed-polarization electro-absorption modulator. IEEE Transactions on Microwave Theory and Techniques, 2011, 59(12): 3239–3248
23. Hraimel B, Zhang X. Suppression of radio over fiber system nonlinearity using a semiconductor optical amplifier and mixed polarization. In: Proceedings of Optical Fiber Communication (OFC) Conference. Anaheim, CA, 2013, Paper JTh2A.59
24. Chen X, Li W, Yao J. Microwave photonic link with improved dynamic range using a polarization modulator. IEEE Photonics Technology Letters, 2013, 25(14): 1373–1376
25. Li W, Yao J. Dynamic range improvement of a microwave photonic link based on bi-directional use of a polarization modulator in a Sagnac loop. Optics Express, 2013, 21(13): 15692–15697
26. Zhu R, Shen D, Zhang X, Liu T. Analysis of dual wavelength linearization technique for radio-over-fiber systems with electro-absorption modulator. IEEE Transactions on Microwave Theory and Techniques, 2015, 63(8): 2692–2702

Xiupu Zhang (M'00–SM'07) received B.Sc. degree from the Harbin Institute of Electrical Technology (now Harbin University of Science and Technology), Harbin, China, in 1983, M.Sc. degree from the Beijing University of Posts and Telecommunications, Beijing, China, in 1988, and Ph.D. degree from the Technical University of Denmark, Lyngby, Denmark, in 1996, all in electrical engineering.

From 1983 to 1985, he worked for manufacturing fibers and fiber cables in China. From 1985 to 1988, he studied for the Master's degree at Beijing University of Posts and Telecommunications, China. From 1988 to 1992, he was engaged in the construction of telecommunication networks in Beijing, China. From 1992 to 1996, he studied for the Ph.D. degree at the Technical University of Denmark. He then spent approximately one and a half years at Chalmers University of Technology, Göteborg, Sweden, where he investigated high-speed fiber-optic transmission. From 1998 to 2002, he worked, as a senior engineer, in the fiber-optics industry, involved in design of repeaterless fiber-optic transmission systems, design of erbium-doped fiber amplifiers and fiber Raman amplifiers, design of optical transmitters and receivers, and design of metropolitan optical networks, in North America including Montreal and Ottawa, Canada, and Piscataway, NJ, USA. In June 2002, he joined Concordia University, Montreal, Quebec, Canada and became an associate professor. Currently, he is a full professor in the Department of Electrical and Computer Engineering, Concordia University. He has authored and co-authored about 200 refereed technical publications, including ~110 journal publications published in IEEE, Optical Society of America, and other related journals, and ~100 conference presentations in IEEE related conferences such as the Optical Fiber Communications Conference.

His current research interests include radio over fiber systems, quantum-dot semiconductor lasers, broadband photodiodes with microwave packaging and mode division multiplexed fiber optic transmission.